Macalester Journal of Physics and Astronomy

Volume 4
Issue 1 *Spring 2016*

Article 11

May 2016

Rotational and Hyperfine Analysis of AuS

Ian A. Wyse
Macalester College, iwyse@macalester.edu

Rotational and Hyperfine Analysis of AuS

Abstract

Gas phase diatomic gold sulfide, AuS, was analyzed using optical spectroscopy. High-resolution spectra were collected and characterized and a global fit of the $A^2\sum^+$-$X^2\prod_{3/2}$ (0,0), $B^2\sum^-$-$X^2\prod_{3/2}$ (0,0), and $C^2\Delta_{3/2}$-$X^2\prod_{1/2}$ (0,0) transitions at 15570 cm^{-1}, 16290 cm^{-1}, and 17670 cm^{-1} was compiled and resulted in rotational constant determinations for the $A^2\sum^+((2\sigma)^1(4\pi)^4)$, $B^2\sum^-((2\sigma)^2(4\pi)^2(2\sigma^*)^1)$, and $C^2\Delta_{3/2}((2\sigma)^2(4\pi)^2(2\sigma^*)^1)$ upper states, as well as the for the $X^2\prod_{3/2}((2\sigma)^2(4\pi)^3)$ ground state. Hyperfine constants were determined for the $A^2\sum^+$ and $B^2\sum^-$ states, but were too small to be resolved in our spectra for the $C^2\Delta_{3/2}$ state and $X^2\prod$ ground state.

Keywords

spectroscopy, diatomic, visible

Rotational and Hyperfine Analysis of AuS

Ian Wyse
Department of Physics and Astronomy
Macalester College, Saint Paul, MN, 55015

ABSTRACT - Gas phase diatomic gold sulfide, AuS, was analyzed using optical spectroscopy. High-resolution spectra were collected and characterized and a global fit of the $A^2\sum^+$-$X^2\prod_{3/2}$ (0,0), $B^2\sum^-$-$X^2\prod_{3/2}$ (0,0), and $C^2\Delta_{3/2}$-$X^2\prod_{1/2}$ (0,0) transitions at 15570 cm^{-1}, 16290 cm^{-1}, and 17670 cm^{-1} was compiled and resulted in rotational constant determinations for the $A^2\sum^+((2\sigma)^1(4\pi)^4)$, $B^2\sum^-((2\sigma)^2(4\pi)^2(2\sigma^*)^1)$, and $C^2\Delta_{3/2}((2\sigma)^2(4\pi)^2(2\sigma^*)^1)$ upper states, as well as the for the $X^2\prod_{3/2}((2\sigma)^2(4\pi)^3)$ ground state. Hyperfine constants were determined for the $A^2\sum^+$ and $B^2\sum^-$ states, but were too small to be resolved in our spectra for the $C^2\Delta_{3/2}$ state and $X^2\prod$ ground state.

I. Introduction:

The Au-S bond is of interest to both computational and experimental physical chemists. For physical chemists, data about the Au-S bond provides complementary analysis for the study of the gold-thiol bond. This bond is the subject of much interest in the growing field of nanomaterial studies [1,2], as gold nanoparticles spontaneously bond with thiol groups in larger structures. This is useful for the creation of self-assembling monolayers (SAMs), materials that spontaneously form on planer gold surfaces. Understanding why thiol groups bond spontaneously to gold particles, while other functional groups do not, is an important step in increasing the diversity of SAMs. While gas phase AuS is not completely analogous to the gold-thiol bond, a better understanding of the gold-sulfur interaction in its most basic form allows for a better understanding of the properties of the bond that lead to its spontaneous formation on gold surfaces.

From a computational standpoint, the Au-S bond is interesting as gold has a large nuclear mass, causing its electrons exhibit relativistic behavior. Accurately modeling of this type of behavior is difficult, but fundamental to determining the characteristics of systems that involve relativistic species. Our research provides empirical data, which can be used to improve theoretical models, not just of gold diatomics, but of all molecules that involve relativistic behavior.

Previous work in our group on the spectra of AuS focused on its vibrational and electronic transitions. This work determined there to be electronic transitions from the $X^2\prod$ ground state to the $A^2\sum^+$, $a^4\sum^-$, $B^2\sum^-$, and $C^2\Delta_i$ upper states. It found the electron configuration of ground state to be $(2\sigma)^2(4\pi)^3$, while the upper state configurations are $(2\sigma)^1(4\pi)^4$ for the $A^2\sum$ state and $(2\sigma)^2(4\pi)^4(2\sigma^*)^1$ for the $a^4\sum^-$, $B^2\sum^-$, and $C^2\Delta_i$ states [3].

Figure 4 depicts the transitions that result in each of the states. This paper focuses on the $X^2\prod$ ground state and $A^2\sum^+$, $B^2\sum^-$, and $C^2\Delta_i$ upper states with the aim to collect high-resolution data in order to determine the rotational and hyperfine parameters that describe the bond.

The rotational and hyperfine spectra of molecules are much more closely spaced than the vibrational and electronic spectra. This is due to much smaller energy spacing between rotational levels. The energy of rotational levels in molecules, is determined by the equation:

$$E(J) = BJ(J+1) - DJ^2(J+1)^2 + HJ^3(J+1)^3,$$

where B is the rotational constant of the bond and J is the rotational energy level of the molecule. The term $BJ(J+1)$ is a calculation of the energy of the rotational level based on a model of the molecule as a rigid rotator. Constants D and H are centrifugal distortion constants, which take into account the fact that molecules are not rigid rotators and that a rotating molecule will have a longer bond length than a stationary one. The centrifugal force of the rotation separates the molecules, changing the total energy of the system.

Hyperfine splitting occurs when rotational energy levels are shifted or degeneracies in rotational levels are separated by a magnetic or electric field created by the nuclear spin of the atoms in the molecule. There are many parameters that govern these small shifts and splits, each resulting in a different perturbation of the levels. The relevant constants in this work are c, the dipole coupling term, eQq_0, the quadrupole coupling term, γ, the nuclear spin-orbit coupling constant, and c_I, the nuclear spin-rotation coupling constant. The electric dipole and quadrupole coupling constants arise because the angular momentum of a rotating nucleus causes an effective electric dipole if

the spin of the nucleus is greater than or equal to 1/2 and an electric quadrupole if its spin is greater than or equal to 3/2. This electric dipole or quadrupole can couple with the charge of unpaired electrons and split the degeneracies of rotational energy levels.

The nuclear spin-orbit coupling and nuclear spin-rotation coupling arise due to magnetic fields caused by the nuclear spin of one or both of the atoms in the molecule. These fields can couple with the orbital angular momentum of a state or the angular momentum of an electron to perturb rotational energy levels. The number of hyperfine lines each rotational transition is split into is determined by the sum of the spins of both nuclei. The sum of the nuclear spins for gold and sulfur is 3/2, so we expected to see rotational lines split into four components, due to the 3/2, 1/2, -1/2, and -3/2 components of the nuclear spin.

II. Methodology:

Laser excitation spectra were collected using a hollow cathode chamber. Molecules were produced by streaming a gaseous mixture of argon and carbonyl sulfide through a 4 mm diameter hole in the center of a 6 mm diameter gold cathode. A 6 mA dc electric discharge was produced between a wire anode approximately 2 cm away from the gold cathode and the cathode itself. A diagram of the cathode is included as figure 5. This resulted in plasma containing rotationally and vibrationally hot (T > 300K) AuS that was then expanded though a 3 mm slit into a vacuum chamber pumped down to 1.6 Torr.

High-resolution spectra were recorded using a single-mode, continuous wave Coherent 899-29 ring laser pumped with a Coherent Verdi V-10 laser. Gas was probed 10 mm away from the slit using intermodulated florescence spectroscopy, a method in

which the laser is split and then double passed horizontally through the chamber. A diagram of this method is included in figure 6. Each half of the laser was chopped at a different frequency and emissions were amplified at the sum frequency of the two choppers in order to reduce noise and eliminate Doppler Broadening in our data, a phenomenon that occurs when molecular transitions appear to be occurring at higher or lower energy than they actually are because molecules are red or blue shifted with respect to the laser. Emissions were also filtered through a red pass filter set to the blue of the laser band in order to block discharge noise. Line widths of approximately 30 MHz were recorded, indicating that the dominate source of noise was power broadening, as the laser has a frequency resolution of ~1MHz. Spectra were recorded using a Hamamatsu R928 photomultiplier tube. Data were calibrated against diatomic, sub-Doppler iodine spectra that were simultaneously collected alongside our AuS spectra.

III. Results and Discussion:

Doubling of each of the branches in the recorded vibrational bands due to lambda doubling and the relatively wide hyperfine spacing in the A-$X_{3/2}$ and B-$X_{3/2}$ transitions made line assignments difficult, as large portions of the spectra were blended despite narrow line widths. Lambda doubling is a phenomenon that occurs because the total electronic angular momentum of a molecule can point either direction down the inter-nuclear axis of the molecule. In each case the angular momentum couples with the nuclear spin, resulting in slightly different energies for the different orientations. If the energy spacing between orientations is large enough, this results in the doubling of each

rotational line, causing each vibrational band to contain two P, Q, and R-branches instead of the usual one.

First and second combination differences, determined though analysis of the ground state, allowed assignments to be made despite blending. Once the process of line assignments was complete, a global fit of the A-$X_{3/2}$, B-$X_{3/2}$, and C-$X_{1/2}$ transitions was performed using a Hamiltonian created by combining Hamiltonians for each of the states. The fitting program performed a least squares analysis of the rotational and hyperfine parameters in each of the states based on the transition energies of all recorded rotational lines and their hyperfine components. The results of this fit are shown in tables 1, 2, 3, and 4.

Both the $B^2\sum^-$ and $A^2\sum^+$ upper states exhibited hyperfine splitting, with the $B^2\sum^-$ state displaying much stronger hyperfine character than the $A^2\sum^+$ state. This can be seen in figures 1 and 2, as each four-peak R, P, or Q line is slightly more than .1 cm^{-1} wide in the $B^2\sum^-$ state (Figure 2), while only .05 cm^{-1} wide in the $A^2\sum^+$ state (Figure 1). This is consistent with the hyperfine constants determined for each state, as γ values, the nuclear spin-rotation coupling constant, c_i, and the electric quadrupole coupling constant, eQq_0, for the $B^2\sum^-$ state were an order of magnitude larger than those of the $A^2\sum^+$ state. The parameter c was included in the fitting of the $B^2\sum^-$ state but not the $A^2\sum^+$ state because its inclusion in the fit for the $A^2\sum^+$ state resulted in a standard deviation for the constant larger than the constant itself.

The $C^2\Delta_{3/2}$- $X^2\prod_{1/2}$ band exhibited little to no hyperfine splitting, as seen in figure 3, indicating that either the hyperfine parameters in the $C^2\Delta_{3/2}$ upper state and ground state perfectly cancel one another, or that neither the ground nor the $C^2\Delta_{3/2}$ upper states exhibit hyperfine splitting. Since previous single band analysis of $A^2\sum^+$-

$X^2\prod_{3/2}$ and $B^2\sum^-$-$X^2\prod_{3/2}$ transitions indicated little to no ground state hyperfine character, we chose to assume that $C^2\Delta_{3/2}$ does not have discernable hyperfine splitting either, and therefore set those parameters to zero during least squares analysis. For that reason, hyperfine parameters were left out of Table 4.

The rotational constant, *B*, for the $A^2\sum^+$ upper state was larger than that of the $C^2\Delta_{3/2}$ and $B^2\sum^-$ states and its centrifugal distortion term, *D*, was smaller, indicating that the molecule's bond length in the $C^2\Delta_{3/2}$ and $B^2\sum^-$ states is longer than in the $A^2\sum^+$ state and that the bond is more flexible. This in turn implies that the $(2\sigma)^2(4\pi)^2(2\sigma^*)^1$ electron configuration, somewhat unsurprisingly, results in a weaker bond than the $(2\sigma)^2(4\pi)^3$ configuration. The energy gap between the 2σ bonding orbital and the 4π nonbonding orbital therefore must be smaller than the gap between the 4π nonbonding and $2\sigma^*$ antibonding orbitals, a conclusion supported by previous electronic work. Additionally, while the rotational constants for the B and C states were very similar, *B* was slightly larger in the C state than in the *B* state. This indicates that placing two electrons in the same orbital is less energetically stable than placing them in separate orbitals in AuS.

Analysis of the $A^2\sum^+$-$X^2\prod_{3/2}$ and $B^2\sum^-$-$X^2\prod_{3/2}$ transitions indicate that hyperfine character in the bond resides in the excited electronic states and that the $X^2\prod_{3/2}$ ground state does not exhibit any hyperfine character. For that reason, hyperfine parameters were left out of the least squared fitting for the ground state as their inclusion resulted in standard deviations that exceeded their values. Analysis of the ground state parameters in our previous work determined the ground state bond length to be 2.156(2) Å and the bond dissociation energy to be 298 ± 2 kJ/mol [3]. The spin-orbit

coupling constant, *A*, was determined from vibrational and electronic analysis so was left constant in the fitting of the rotational and hyperfine parameters.

IV. Conclusion:

We recorded high-resolution spectra from the $A^2\sum^+$-$X^2\prod_{3/2}$ (0,0) band located at 15570 cm^{-1}, the $B^2\sum^-$-$X^2\prod_{3/2}$ (0,0) located at 16290 cm^{-1}, and $C^2\Delta_{3/2}$-$X^2\prod_{1/2}$ (0,0) located at 17670 cm^{-1}. We then assigned rotational and hyperfine values to each peak in the spectra and preformed a least squares fitting based Hamiltonians for each of the states. This least squares fitting resulted in the rotational and hyperfine constant values found in tables 1-4. The $B^2\sum^-$-$X^2\prod_{3/2}$ state was found to have the greatest hyperfine character and therefore the hyperfine parameters of the $B^2\sum^-$ state had the greatest magnitude. The $A^2\sum^+$ state had splitting parameters an order of magnitude smaller than in the $B^2\sum^-$ state and the $C^2\Delta_{3/2}$ state and $X^2\prod$ ground state had no discernable hyperfine character.

V. Future Work:

Future work in the Varberg group includes high-resolution analysis of the remaining $a^4\sum^-$ upper state and the recording and investigation of additional transitions to the electronically hot $X^2\prod_{1/2}$ ground state: specifically the $A^2\sum^+$-$X^2\prod_{1/2}$ and $B^2\sum^-$-$X^2\prod_{1/2}$ transitions seen in vibrational work. Beyond AuS, the group intends to investigate the spectra of AgS at both low and high resolution, as Au and Ag are in the same group, so properties of the two molecules should be similar and comparison of the two bonds should help characterize how the properties of atoms change throughout the Cu-Ag-Au group.

VI. References:

(1) Azcarate, J.C.; Corthey, G.; Pensa, E. ;Vericat,C.; Fonticelli,M. H.; Salvarezza, R. C.; Carro, P. Understanding the surface chemistry of thiolate-protected metallic nanoparticles. *J. Phys. Chem.* Lett. **2013**, 4, 3127−3138.

(2) Häkkinen, H. The gold–sulfur interface at the nanoscale. *Nat. Chem.* **2012**, 4, 443-455.

(3) Kokkin, D.; Zhang, R.; Steimle, T.; Wyse, I.; Pearlman, B.; Varberg, T. Au–S Bonding Revealed from the Characterization of Diatomic Gold Sulfide, AuS. *Journal of Physical Chemistry.* 2015. 119 (48), 11659-11667.

TABLE 1: Constants (in cm^{-1}) for the $X^2\Pi$ (v = 0) ground state of AuS

	Value	σ
B	0.130389	5.25×10^{-6}
D	4.05×10^{-8}	3.195×10^{-9}
H	-2.5×10^{-12}	6.5×10^{-13}
A	-131.85	–
p	1.525×10^{-2}	2.05×10^{-5}
p_D	1.3×10^{-8}	8.6×10^{-9}
c	2.1×10^{-2}	3.4×10^{-3}
A_D	2.3218×10^{-3}	4.937×10^{-6}

Note: Values not calibrated with I_2

TABLE 2: Constants (in cm^{-1}) for the $A^2\Sigma^+$ (v=0) excited state of AuS

	Value	σ
T_e	14898.3	3.283×10^{-4}
B	0.12763	4.88×10^{-6}
D	1.8×10^{-8}	3.82×10^{-9}
H	-1.15×10^{-11}	1.189×10^{-12}
γ	-8.08×10^{-2}	4.41×10^{-5}
γ_D	1.17×10^{-6}	1.11×10^{-7}
γ_H	-4.47×10^{-10}	6.65×10^{-11}
b_F	7.051×10^{-2}	1.66×10^{-4}
c_I	1.26×10^{-5}	3.90×10^{-6}
eQq_0	9.453×10^{-3}	7.231×10^{-4}

Note: Values not calibrated with I_2

TABLE 3: Constants (in cm^{-1}) for the $B^2\Sigma^-$ (v=0) excited state of AuS

	Value	σ
T_e	15628.9	3.895×10^{-4}
B	0.12347	4.75×10^{-6}
D	2.75×10^{-8}	3.08×10^{-9}
γ	0.1232	3.618×10^{-3}
γ_D	-1.39×10^{-5}	1.55×10^{-7}
γ_H	1.58×10^{-9}	1.31×10^{-10}
b_F	0.124	3.61×10^{-3}
c	0.38	1.07×10^{-2}
c_I	4.436×10^{-4}	5.92×10^{-6}
eQq_0	-1.394×10^{-2}	8.585×10^{-4}

Note: Values not calibrated with I_2

TABLE 4: Constants (in cm-1) for the $C^2\Delta_{3/2}$ excited state of AuS

	Value	σ
T_e	18325.9	3.938×10^{-4}
B	0.12476	6.95×10^{-6}
D	5.15×10^{-8}	3.03×10^{-9}
H	-2.7×10^{-12}	5.85×10^{-13}

Note: Values not calibrated with I_2

Figure 1: Spectrum for the $A^2\sum^+$-$X^2\prod_{3/2}$ (0,0) transition of AuS. Two R-branches are visible, as well as one of the R-heads.

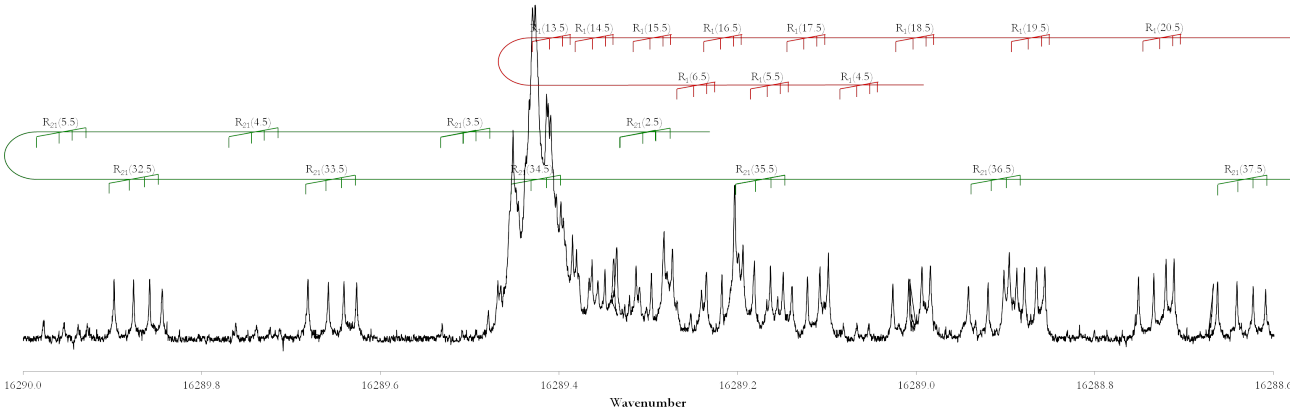

Figure 2: Spectrum for the $B^2\sum^-$-$X^2\prod_{3/2}$ (0,0) transition of AuS. Four branches a visible: two P-branches, one R-branch, and one Q-branch.

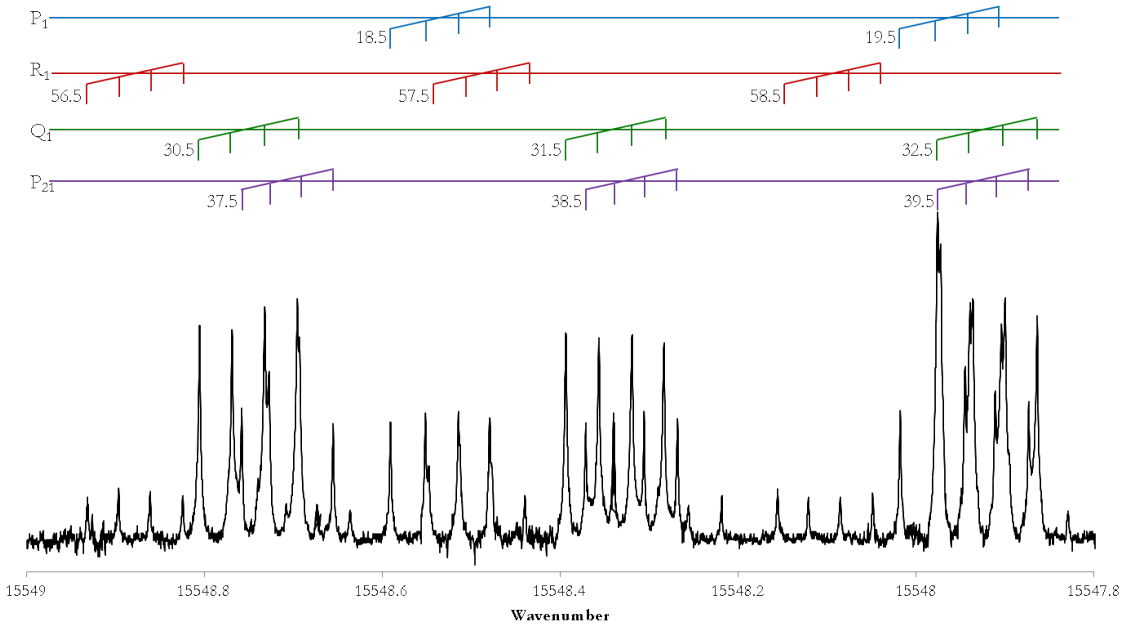

Figure 3: Two halves of the spectrum of the $C^2\Delta_{3/2}$-$X^2\prod_{1/2}$ (0,0) transition for AuS. All six branches are visible in the spectrum. No hyperfine splitting of rotational lines is apparent.

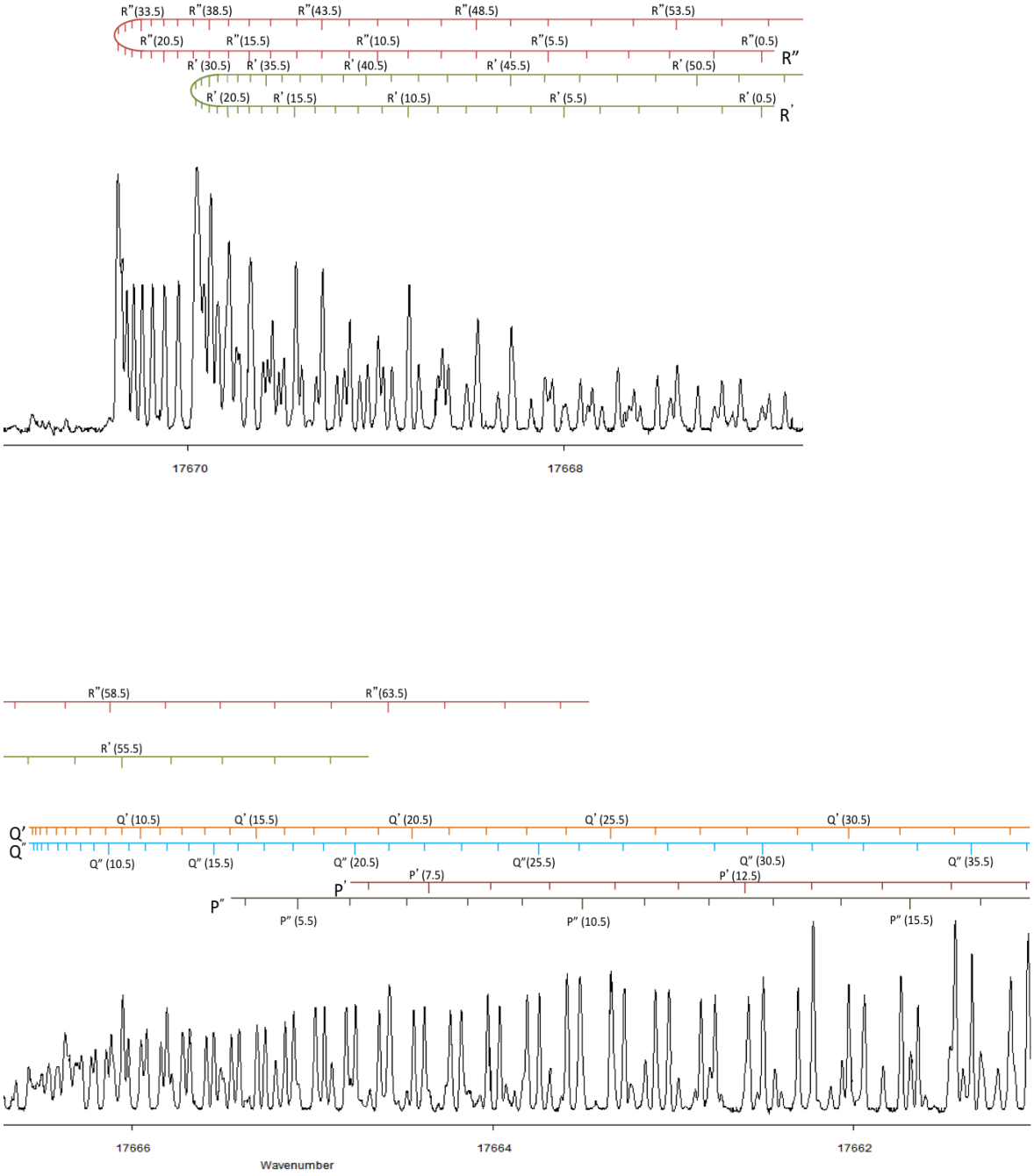

Figure 4: Diagram of electronic transitions found in AuS.

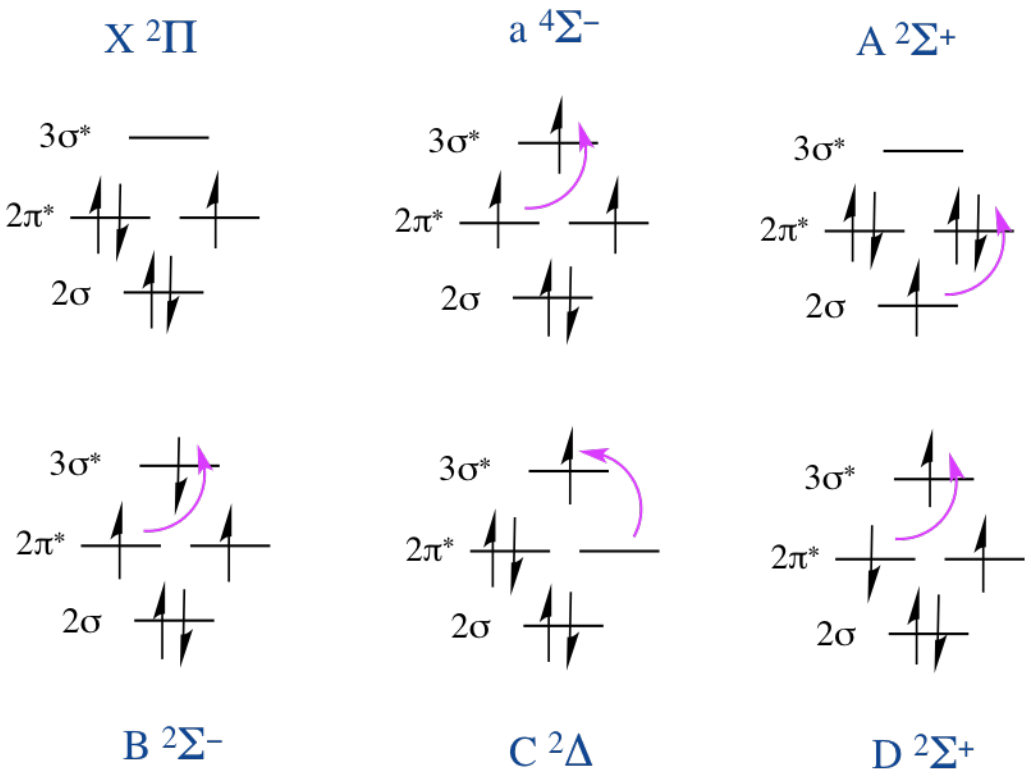

Figure 5: Illustration of sample syntheses through hollow cathode techniques.

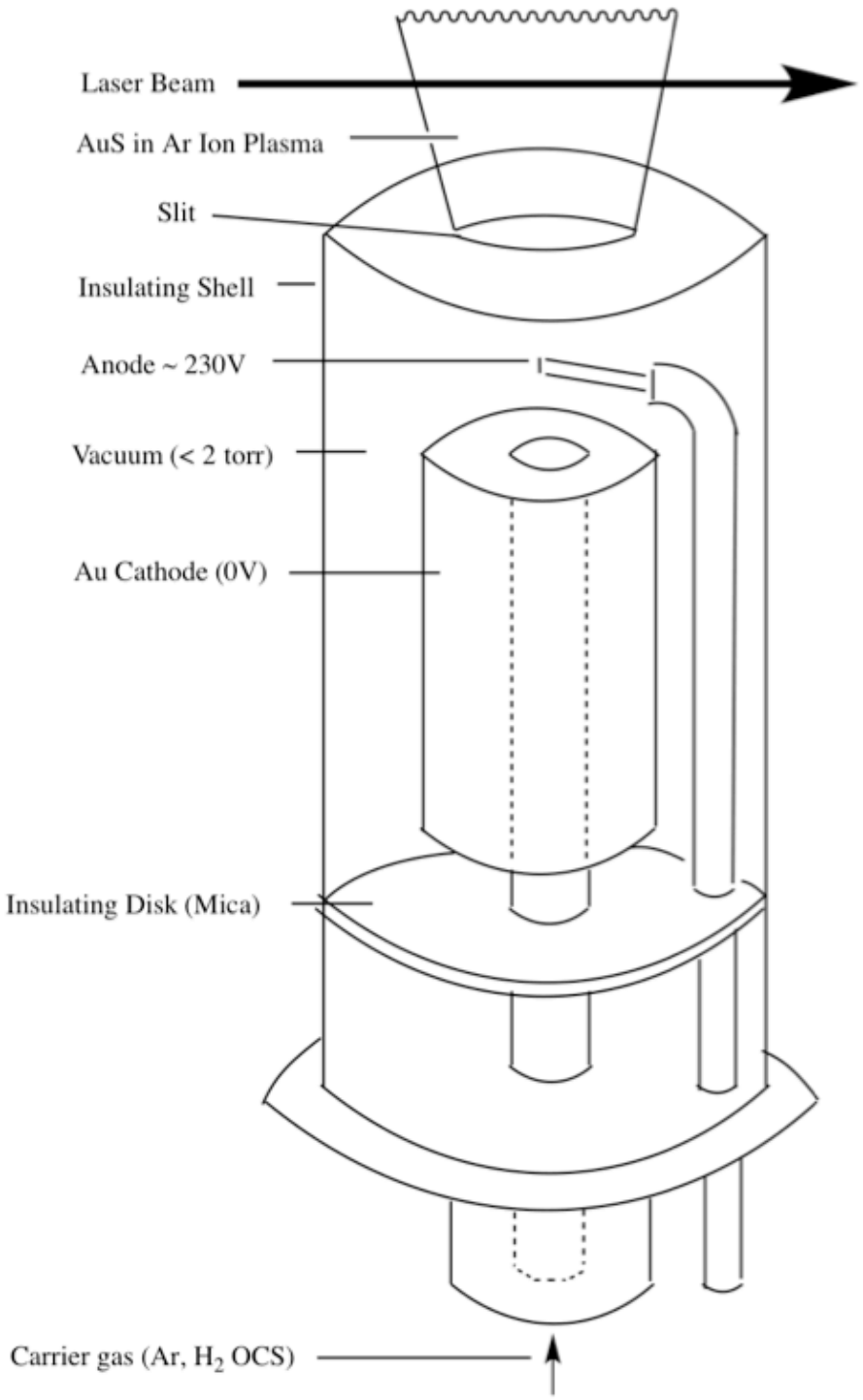

Figure 6: Diagram of method of intermodulated florescence of spectroscopy.